Czesław Machelski
Prof. dr hab. inż.
Politechnika Wrocławska
Wydział Budownictwa Lądowego i Wodnego
Katedra Mostów i Kolei
czeslaw.machelski@pwr.edu.pl

Piotr Tomala
Mgr inż.
ViaCon Polska Sp. z o.o.
piotr.tomala@viacon.pl

DOI: 10.35117/A_ENG_21_09_02

Expanded range of testing of soil-steel bridge with use moving loads

Abstract: In this paper the results of the live load tests of soil steel bridge are presented. The structure was designed with use of the largest possible corrugation type UltraCor. Parameters of analysed structure were referred to the current record structures in the term of span. Standard test procedure have been expended to check the efficiency of the position-changing loads i.e live loads but in a quasi-static approach. The measuring base was the upper part of the shell periphery equipped with inductive and dial gauges to determine deflections at regular layout. Paper presents another example of the formation of "hysteresis loop" where the live load is passing back and forth along the same path. In the case of a dense layout of measuring points it is possible to use a differential algorithm to estimate the bending moments in corrugated steel plates. Analysed case shows that the internal forces and displacements due to the live loads are much smaller than during construction. The purpose of the paper is to indicate the specific behaviour of soil-steel structures in relation to classical arch bridges.

The rigidity of corrugated sheeting

The paper presents the methodology and results of testing a typical bridge structure made of corrugated steel, as shown in Fig. **1**. A characteristic feature of the structure of these structures is the formation of many times greater internal forces and displacements during their construction than when used as road and railway bridges [1, 3, 4, 5, 6, 8, 9, 12, 13]. After assembly, the corrugated sheet coating is very flaccid. It is subject to significant deformation during placing the backfill [13]. For these reasons, objects with large spans are monitored during the construction phase, using geodetic techniques [1, 3, 12, 13]. It is only during use that the corrugated sheet coating as a structure immersed in the soil medium, in a ready object, is characterized by high stiffness [11, 14]. A characteristic feature of soil-shell structures, unlike classic arched bridges, is the large impact of the soil backfill and road surface on the load capacity of the structure [14, 15].

In the analyzed object, as a supplement to the classic acceptance tests of bridge structures, measurements of deflections under the load changing the position were carried out. Due to the small values of displacements under operational loads, it is necessary to use inductive or dial sensors with a measurement accuracy of up to 0.01 mm. From such results, one can also evaluate the bending moments as in the algorithm given in the paper. Obviously, measurements with the use of strain gauges glued to a corrugated sheet are much more effective [2, 3, 5, 9]. However, this involves the use of specialized measuring equipment and the preparation of the measuring base. For this reason, such research methodology is used for objects with the largest spans [5, 7, 9] as in shells with geometrical parameters listed in the tab. **1**.

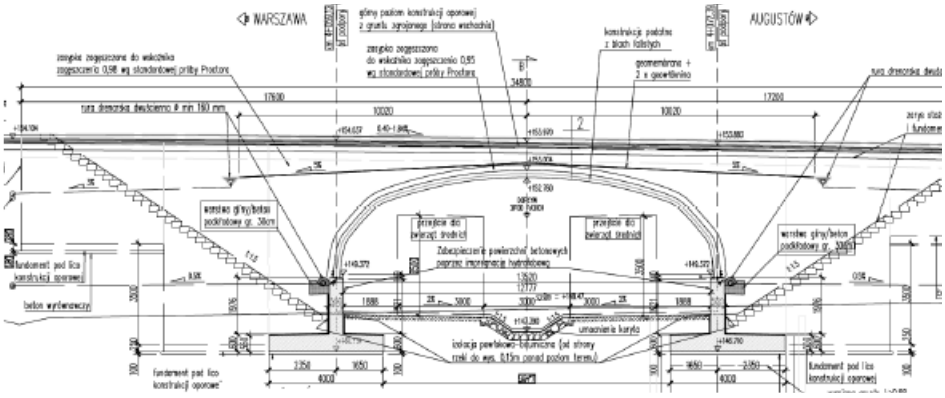

1. Cross-section of the analyzed object in the Szczuczyn bypass

Examples of objects listed in Table **1** are of similar shape and similar proportions of dimensions intended for communication as road objects. The largest span structure in the world was built at Ras Al Khajmah near Dubai at United Arab Emirates [1]. The facility in Ostróda is the second largest facility in the world built in Poland [1]. The third facility analyzed in the study was built along the Szczuczyn bypass. It is characterized by a much smaller span than the record-breaking ones made of sheets of the same profile - UltraCor. A special feature is the small thickness of the backfill with the base and surface of 1.03 m.

Tab. 1. Geometric parameters of the analyzed shells

Object	Shell's dimensions [m]			Type of sheet metal ***a*×*f*×*t***	***EI/a*** MNm^2/m	k_m kN/m
	L	***H***	***R***			
Szczuczyn	13,276	3,630	14,376	UC 500×237×5	5,704	32.4
Ostróda	25,724	9,110	16,632	UC 500×237×9,65	19,89	27.8
Dubai	32,660	9,570	29,680	UC 500×237×12	22,80	21.7

The characteristic geometrical parameters of the shells are their span **L**, height **H** and the radius of curvature of the upper part of the shell **R**, presented in tab. **1**. Fig. **2** shows the geometry of the corrugated sheet used in the buildings, with the characteristic dimensions UC ***a*×*f*×*t***, as in tab. **1**. The **EI** value is the bending stiffness of the coating usually related to the wavelength ***a***.

The design guidelines and technical recommendations define the minimum installation stiffness of the coatings in the form of a parameter, as in the formula

$$k_m = \frac{EI}{a \cdot L^2} \quad . \tag{1}$$

The values obtained in the analyzed coatings are summarized in the last column of tab. **1**. For lower profile coatings, lower k_m values are used. For example, when the coating is made of MP 200×55×8 [mm] sheet with a span of **L** = 11 m, the value k_m = 6.25 kN/m is obtained from the formula (1). A parameter similar to k_m is used in the case of constructed facilities - it takes many times greater values [11, 14].

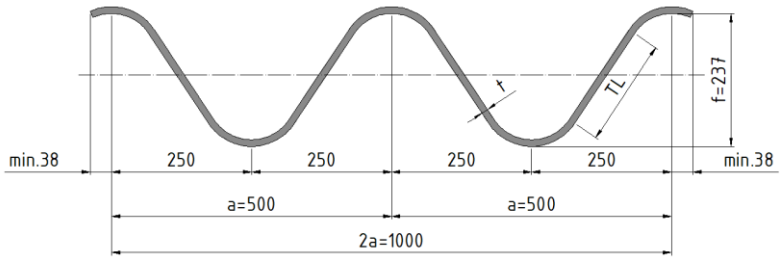

2. The geometry of the UC 500 × 237 × 8 corrugated sheet [mm]

Coating deflection during car travel

In the study of arch-shaped bridge structures under moving load, their specific characteristics are used - minimal dynamic effects. Thanks to this, in the vaulted bridges it is possible to analyze displacements in a quasi-static approach, also during operational runs of freight trains when the speeds reach the value of v = 20 m/sec. In the case of soil-shell structures, the dynamic effects are also small but greater than in the previous ones [15]. For this reason, in the presented tests, vehicle speeds of a few m/sec were used.

A car with front axle loads $\boldsymbol{P}_1 = \boldsymbol{P}_2 = 70$ kN and rear axles $\boldsymbol{P}_3 = \boldsymbol{P}_4 = 90$ kN is used in the tests given in the paper. The vehicle geometry is the wheelbases: $\boldsymbol{a}_{12}$ =1,2 m $\boldsymbol{a}_{23}$ = 3,0 m and $\boldsymbol{a}_{34}$ = 1,8 m. The measurement line is a system of points regularly spaced on the circumferential band of the shell with a spacing of $\boldsymbol{c}$ = 1,2 m car axle positions are shown in Fig. **3.**

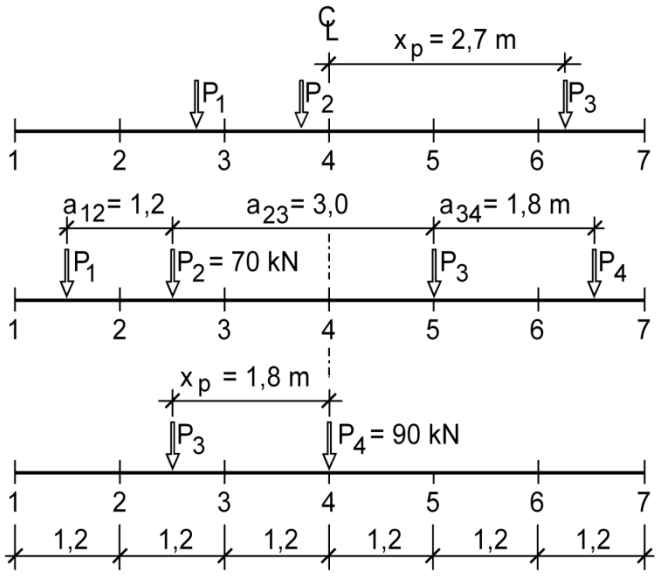

3. Diagram of the measuring system and loads

The journeys of the car took place from W (Warsaw) to A (Augustów) with driving forward, and in the case of A - W backwards along the same line of traffic. Thus, in any vehicle position defined by the $\boldsymbol{x}_p$ coordinate, the vehicle positioning is identical, regardless of the direction of travel A - W or W - A. Fig. **4** shows the results of measuring the deflections of three selected points 2, 4 (shell key), 6. Coordinate $\boldsymbol{x}_p$ defines the position of axis 3 from the shell key (axis 3 is closest to the vehicle's center of gravity: 1.07 m). In the tests of the sectional car journey, it was stopped at $\Delta\boldsymbol{x}_p$ = 1.5 m for taking readings from measuring devices. The journey started at its position $\boldsymbol{x}_p$ = -10.8 m, and the return when $\boldsymbol{x}_p$ = 14.7 m

a) point 2 from fig. 3

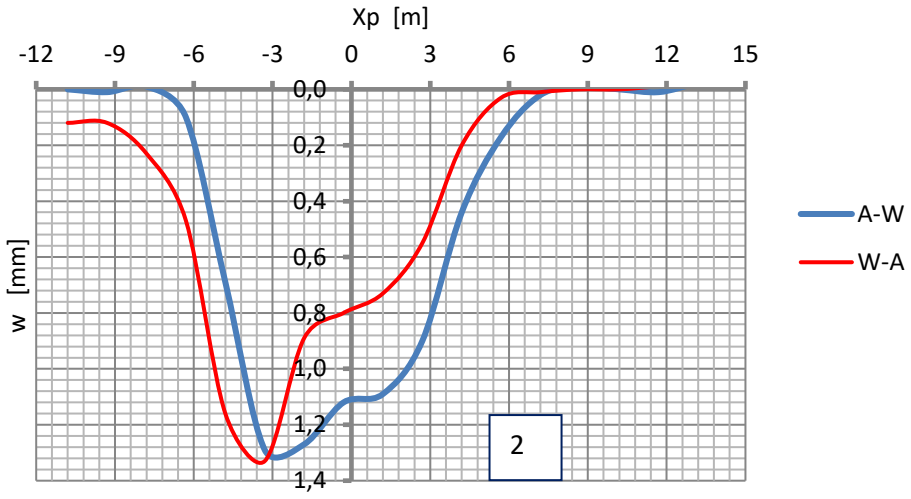

b) point 4 (key) from fig. 3

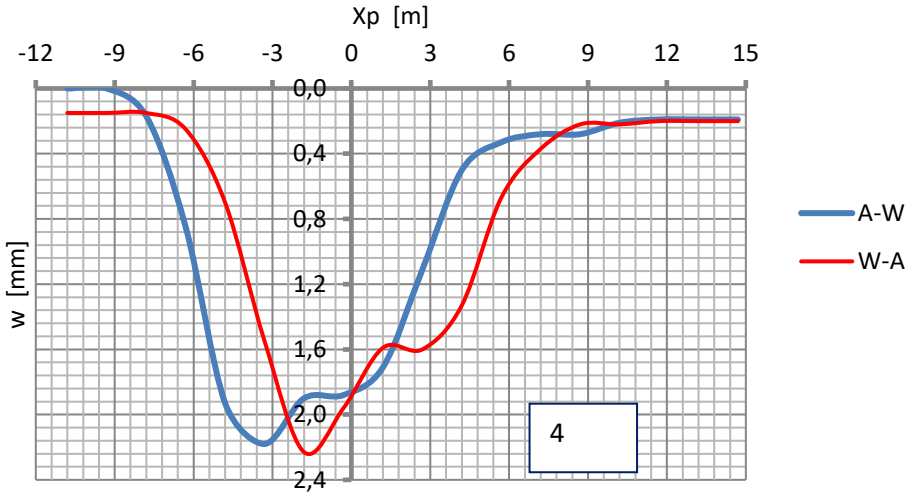

c) point 6 from fig. 3

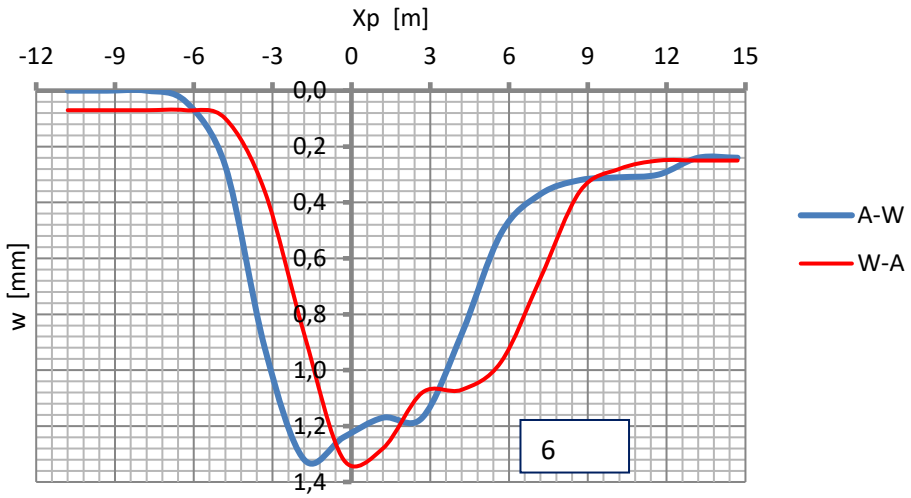

4. Changes in the deflections of the coating measurement points during the intermittent run of the car

When driving in both directions, two lines of deflection are created with a common point at the end of the original travel and the beginning of the U-turn. A characteristic result of this research methodology is the appearance of advance on the deflection diagram, visible from the comparison of the results for symmetrically located points 2 and 6. It depends on the direction of the car! This phenomenon has been observed for a long time [9] - it is a specific feature of soil-shell objects. This effect cannot be registered during the continuous run shown in Fig. **5**. After the full load cycle - two passes over the coating, there are relatively small residual displacements. During the drive with segment breaks, during the measurement period of 27 minutes, 35 measurement readings were taken.

5. Changes in the deflections of the coating measurement points during continuous driving of the vehicle

Fig. **5** shows the deflection changes, but during continuous, uninterrupted driving of the car and not in step terms, as before. Thus, on the horizontal axis, the measurement is the time function and not the vehicle position, as in Fig. **4**. In the time interval 0.28 - 0.45 min. There was an initial run over the shell. During the next 16 seconds, there was a short stop on the other side of the facility. Then the secondary and return run over the coating was then carried out in the time interval of 1.02 - 1.17 min. In this case, the speeds were increased from 1.5 m/sec compared to 1 m/sec during the primary weir. The velocities were estimated based on the characteristic changes in displacements presented in Figures **4** and **5**. A comparison of these graphs shows their great similarity. However, both results were obtained in the next measurement cycle. The journeys over the coating were carried out at different speeds.

The diagrams in Fig. **5** show the starting displacement, the parking displacement in the middle part and the last displacement ending the load cycle. Thus, the actual displacements due to shell deformation should be corrected (zeroed). The double pass over the coating took less than a minute.

Changes in the curvature of the circumferential band of the shell

On the basis of the deformation of the coating shown in Fig. **6**, the change in the curvature of the circumferential strip of the coating can be calculated, e.g. using the finite difference method MRS [10]. It is determined at the midpoint of K on the basis of displacements in the radial direction **r** of neighboring points A and B from the general dependence [10]

$$\kappa_K = \frac{1}{s^2}\left\{ r_A - \left[2 - \left(\frac{s}{R} \right)^2 \right] r_K + r_B \right\} \quad . \tag{2}$$

In formula (2), the values of s are the distance between point K and points A or B. So in this case, s is the length of the segment of a circle with radius $\boldsymbol{R}_w$ as in the formula

$$s = \varphi_w \cdot R_w \quad . \tag{3}$$

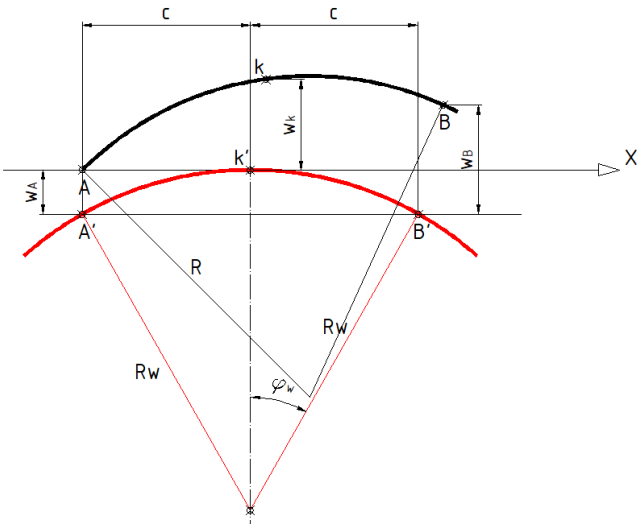

6. Changes in the geometry of the circumferential sector of the shell in the key area

The radius of curvature of the circumferential band of the shell $\boldsymbol{R}_w$ results from its deformation when **r** are displacements in the direction consistent with this radius [6, 10].

In the case when the radius of curvature $\boldsymbol{R}_w$ is very large in relation to **s** in formula (2), simplifications can be applied to the form

$$\kappa_K = \frac{1}{c^2}\{w_A - 2 \cdot w_K + w_B\}, \tag{4}$$

It results from the proportion value, as in the analyzed case

$$\left(\frac{s}{R}\right)^2 = \left(\frac{1{,}212}{14{,}376}\right)^2 = 0{,}007 \quad . \tag{5}$$

Moreover, in formula (4) it is assumed that **s** ≈ **c** and **w** ≈ **r**. Thus, in (4) there is an approach to the equation used in the finite difference method as in the case of a straight bar [10].

The dependence of the bending moment on the change in curvature

The change in curvature, previously defined as the transformed deflection measurement result, is related to the bending stiffness of the corrugated sheet **EI** (see Table **1**) in the bending moment equation, as in the formula

$$M = EI \cdot \kappa \quad . \tag{6}$$

The changes in the curvature κ are calculated from formula (4) on the basis of the deformation of the upper segment of the circumferential band of the shell. Based on the changes in the curvature of κ, it is also possible to determine the normal stresses due to bending from the formula

$$\sigma(M) = \frac{f+t}{2} E \cdot \kappa \quad . \tag{7}$$

With a constant value of **E** = 205,000 MPa, a direct dependence on the geometry of the corrugated sheet ***a*×*f*×*t*,** is visible, as shown in Fig. **2** and Tab. **1**.

Fig. **7** shows diagrams of bending moments along the length of the analyzed section of the circumferential strip. Three settings of the car were assumed while it was traveling in the natural direction (forward), i.e. W-A. One figure shows two plots of $\boldsymbol{M}(x,x_p)$ and $\boldsymbol{w}(x,x_p)$. In this case, it should be emphasized that the function of bending moments **M** strongly depends on the shape of the function **w**. For this reason, the smoothing process $\boldsymbol{w}(x)$ was used in the calculations, assuming an additional intermediate point between the measurement points.

a) x_p = 2.7 m

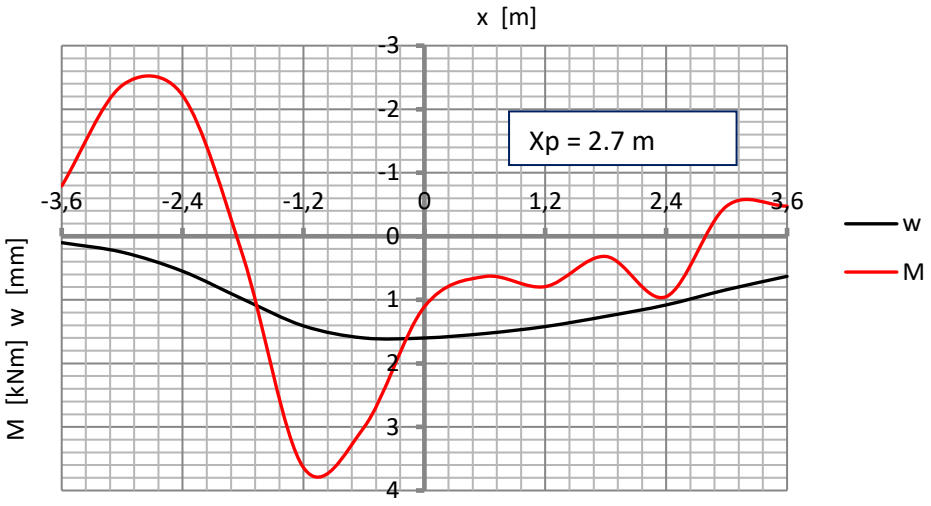

b) x_p = 1.2 m

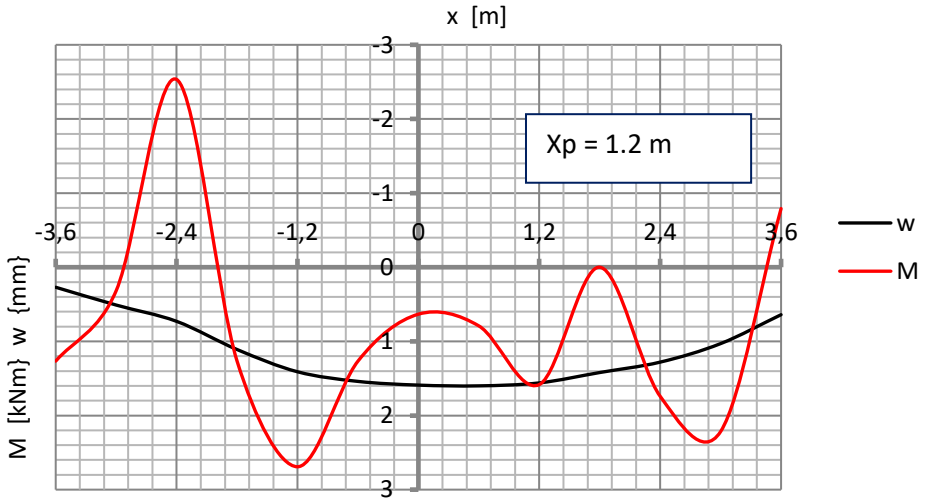

c) x_p = - 1.8 m

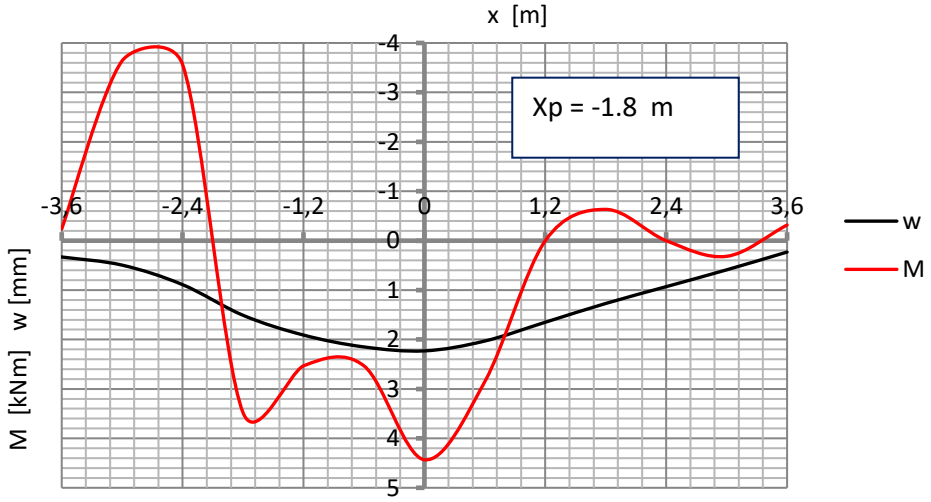

7. Diagrams of bending moments in the circumferential band of the key area

In Tab. **2**, the values characteristic for the analyzed objects from tables 1 obtained from their construction phase. They were calculated for a special construction situation when the backfill level reached the key, i.e. when $\boldsymbol{z}_g = \boldsymbol{H}$. The bending moments were obtained from the formula (6). The values of the bending moments are relatively even in all shells. The dependence of the change in curvature κ and moments **M** on the uplift **w** is not visible. The remaining data shows that the shell geometry undergoes much greater deformation during construction than under a moving load.

Tab. 2. List of calculation results for the analyzed objects

Object	$\boldsymbol{w}$ [mm]	κ_ε *10^{-3} [1/m]	$\boldsymbol{R}_w$ [m]	$\boldsymbol{M}$ [kNm]
Szczuczyn	82	9.71	12.119	46.3
Ostróda	211	7.04	14.889	70.0
Dubai	92	5.36	25.604	61.1

Summary

The deformation of the coating during the laying of the backfill in the soil and coating structure made of corrugated sheets is significant and can be controlled with the use of geodetic techniques. In the case of operational loads, the displacements and internal forces are much smaller. For this reason, it is useful to use strain gauge measurements that directly determine internal forces, but also displacements [2]. The paper presents an example of using the measurement of displacements to determine bending moments. In this case, it is necessary to use inductive or dial gauges with a measurement accuracy of up to 0.01 mm. In a situation where there is a small thickness of the backfill with the base and surface of 1.03 m, as in the analyzed structure, a dense grid of measurement points is necessary. This allows for the representation of the complex form of the bending moment function.

The paper presents another example of the formation of a "hysteresis loop" in the case of using the moving load cycle, in which the primary run over the object with a reversal along the same path is carried out. The presented analysis methodology is also used to determine the stiffness of bridge structures [11, 14]. The research conducted so far shows that the analyzed objects are analogous to road and rail concrete and steel bridges. At the same time, they are characterized by a very low dynamic excitation [15].

Source materials

[1] Machelski C., Mońka M, Tomala P.: Monitoring of soil-steel structures during construction. Journal of Current Construction Issues. 2019 p. 159-168.
[2] Machelski C.: Soil-steel shell structure displacements functions based on tensometric measurements. Studia Geotechnica et Mechanica Vol. 42 2018 p. 55-57.
[3] Korusiewicz L.: Verification of the method of estimating bending moments in soil-steel structures on the basis of shell deformation. Roads and Bridges 15 (2016) p. 221-230.
[4] Machelski C., Janusz L., Czerepak A.: Estimation of Stress level in the Corrugated Soil-Steel Structures Based on Deformations in the Crown. Journal of Traffic and Transportation Engineering 4(2016) p. 186-193.
[5] Asp O., Laaksonen A.: Instrumentation and monitoring of large-span culvert built under railway in Finland. Archives of Institute of Civil Engineering, 23 2017 p. 53-60.
[6] White K, Sargand S, Massada T.: Evaluation of load rating procedure for metal culverts under shallow soil covers. Archives of Institute of Civil Engineering 23 2017 pp. 311-323.

[7] Moor J., Brachman R.: Research advancing the design of large span deep corrugated metal culverts. Archives of Institute of Civil Engineering 12 2012 pp. 9-19.
[8] Machelski C., Janusz L.: Application of Results of Test in Developing 2D Model for Soil-Steel Railway Bridges. Journal of Transportation Research Board. Vol. 2656:53-6 January 2017.
[9] Machelski C., Tomala P.: Investigation of displacements functions in soil-steel bridge structure based on tensometric measurements. 9th Symp. Steel Bridges, Praga, 10-11 September 2018, p. 18-
[10] Machelski C.: The use of the collocation algorithm for estimating the deformations of soil-shell objects made of corrugated sheets. Studia Geotechnica et Mechanica Vol. 46 2019.
[11] Machelski C.: Stiffness of railway soil-steel structures. Studia Geotechnika et Mechanica. No. 4/2015 p. 29-36.
[12] Machelski C.: Klasyfikacja obiektów gruntowo-powłokowych z uwagi na zmiany deformacji powłoki podczas budowy. Przegląd Komunikacyjny 9/2016 s. 5-10.
[13] Machelski C.: Budowlane obciążenia podatnych obiektów inżynierskich. Przegląd Komunikacyjny 10 (2018) s. 30-35.
[14] Machelski C.: Sztywność obiektu mostowego jako parametru użytkowego konstrukcji inżynieryjnych. Przegląd Komunikacyjny 2/2016 s. 27-32
[15] Machelski C.: Oddziaływania pojazdu na powłokę w obiektach gruntowo-powłokowych. Przegląd Komunikacyjny 9/2017 s. 5-10.